13,07

The effect of sol-gel-synthesis temperature on the structure and magnetic properties of Sr-substituted $La_{0.5}Sr_{0.5}FeO_{3-\gamma}$

© V.D. Sedykh[1], O.G. Rybchenko[1], V.S. Rusakov[2], A.M. Gapochka[2], A.I. Dmitriev[3], E.A. Pershina[1], S.V. Zaitsev[1], K.P. Meletov[1], V.I. Kulakov[1], A.I. Ivanov[1]

[1] Osipyan Institute of Solid State Physics RAS, Chernogolovka, Russia
[2] Moscow State University, Moscow, Russia
[3] Federal Research Center of Problems of Chemical Physics and Medicinal Chemistry RAS, Chernogolovka, Russia

E-mail: sedykh@issp.ac.ru

Received December 27, 2024
Revised December 28, 2024
Accepted December 31, 2024

The effect of temperature used at the final stage of sol-gel synthesis method on the structure, Fe valence states, and Néel temperature of Sr-substituted $La_{0.5}Sr_{0.5}FeO_{3-\gamma}$ has been studied using transmission electron microscopy, X-ray diffraction, Mössbauer and Raman spectroscopy, as well magnetic measurements. The samples were synthesized by sol-gel method in air at the temperatures of 1100 and 1300°C and then annealed in the vacuum in the temperature range of 200–650°C to deoxygenize and deoxidate Fe. Oxygen yield and transition from Fe^{4+} to Fe^{3+} under vacuum annealing have been found out to occur slower in the samples synthesized at higher temperature. Therefore the transformation of the initial rhombohedral phase to the cubic one finishes at the higher annealing temperature. This is explained by the difference in the sizes of the initial crystals formed at different synthesis temperatures. After long final annealing at 650°C, the samples become single-phase with a cubic structure in both cases. It is confirmed by the results of Mössbauer and Raman spectroscopy as well magnetic measurements. The Néel temperatures have been determined for all samples under study. The results obtained by all used methods correlate well between themselves.

Keywords: orthoferrites, Fe valence states, oxygen vacancies.

DOI: 10.61011/PSS.2025.01.60603.356

Introduction

Perovskite orthoferrites $R_{1-x}A_xFeO_{3-\gamma}$, where R is a rare earth element, A is Ba, Ca, or Sr, are promising materials for a wide variety of applications due to their unusual electrical, magnetic, and catalytic properties, for example, as electrode materials for fuel cells, catalysts, chemical sensors, optoelectronic devices, magnetic memory devices, etc. [1,2]. They also exhibit antibacterial properties [3]. To understand the processes occurring in these compounds, it is necessary to know how the substitution of elements, synthesis conditions (synthesis atmosphere, temperature, cooling rate) affect the structure and certain physical properties. Very small changes in synthesis conditions can lead to significant changes in properties. Fe transition metal ions have mixed valence states in these systems, Fe^{3+} and Fe^{4+}, which can be caused by the introduction of divalent ions (A) into the places of a trivalent element (R), and the formation of oxygen vacancies [4].

The impact of the final annealing temperature of sol-gel synthesis on the structure and magnetic properties in Sr-substituted lanthanum ferrite $La_{0.5}Sr_{0.5}FeO_{3-\gamma}$, as well as their evolution during vacuum annealing, has been studied in this paper.

1. Experiment

The initial polycrystalline samples $La_{0.5}Sr_{0.5}FeO_{3-\gamma}$ (50Sr) were obtained by the sol-gel method in air. Lanthanum nitrate $La(NO_3)_3 \bullet 6H_2O$, strontium nitrate $Sr(NO_3)_2$, iron nitrate $Fe(NO_3)_3 \bullet 9H_2O$ in stoichiometric ratio and glycine were used as starting materials for the synthesis by nitrate-glycine method. Metal nitrates and glycine were dissolved in distilled water with intensive stirring until a homogeneous solution was formed. The resulting solution was evaporated at a temperature of 250°C using a laboratory electric stove. Next, the precursor was ground in an agate mortar and annealed at a temperature of 800°C for 5 hours in the air. The annealed powder was ground for 3 hours in a zirconium container of a planetary ball mill with the addition of ethyl alcohol. The final 20-hour annealing of the powders was performed at temperatures of 1300 and 1100°C in the air, followed by slow (together with the oven) cooling to room temperature. The oxygen composition of $La_{0.5}Sr_{0.5}FeO_{3-\gamma}$ was changed by vacuum annealing (10^{-3} Torr) in the temperature range of 200–650°C with a duration of 4 hours for samples 50Sr–1100C and 8 hours for samples 50Sr–1300C. The extended duration of vacuum annealing of sample 50Sr–1300C was chosen to ensure

Abbreviations used in the paper

Samples	Abbreviations
The initial sample synthesized at a temperature of 1100°C	50Sr−1100C
The initial sample synthesized at a temperature of 1300°C	50Sr−1300C
Initial sample annealed in vacuum (AV — annealing in vacuum) at a temperature of 650°C (650AV) with 8-hour annealing	50Sr−1300C−650AV−8h
Initial sample annealed in vacuum (AV — annealing in vacuum) at a temperature of 650°C (650AV) with 10-hour annealing	50Sr−1300C−650AV−10h

the most complete removal of oxygen from crystals, the size of which, and, consequently, the diffusion paths in them, are almost an order of magnitude larger than the corresponding values in sample 50Sr−1100C. This was shown by transmission electron microscopy and will be demonstrated below. In addition, the samples were additionally vacuum annealed at 650°C for 10 hours. The abbreviations used in the paper are listed in the table.

The morphology and average size of the particles and their agglomerates were studied by transmission electron microscopy (TEM). The samples for electron microscopy were prepared as follows: the studied powders were stirred in alcohol by ultrasonic waves for 2 minutes. The resulting suspension was applied to supporting copper grids with a pre-sprayed thin carbon film. 200 kV accelerating voltage was used for the study. The average size of particles and agglomerates was determined from dark-field TEM images. The mapping was performed in TEM using the energy dispersive spectroscopy (EDS) method to characterize the elemental composition of the studied samples.

Structural qualification of polycrystalline samples was conducted at room temperature using Rigaku smartLAB SE diffractometer with CuK_α-radiation. Powder Cell 2.4 and Match3 programs were used for phase analysis and determination of structural parameters.

The Mössbauer measurements of polycrystalline samples were conducted at room temperature and at 85 K using SM 1101 spectrometer operating in constant acceleration mode. A radioactive source ^{57}Co(Rh) was used for the experiment. The spectra were processed and analyzed using the methods of model interpretation and reconstruction of the distribution of hyperfine spectral parameters using SpectrRelax program [5].

Raman scattering spectroscopy (RSS) of polycrystalline samples was performed at room temperature. The RS spectra were measured in the backscattering geometry using a setup consisting of ActonSpectraPro-2500i spectrograph with Pixis2K CCD detector cooled to −70°C and an Olympus microscope. The RS spectra were excited using a continuous solid-state diode-pumped laser with $\lambda = 532$ nm. The laser beam was focused on the sample by Olympus 50× lens in a spot with a diameter of $\sim 3\,\mu$m. The laser radiation line in the scattered beam was suppressed using an edge filter for $\lambda = 532$ nm with an optical density of OD = 6 and the transmission-band edge of $\sim 100\,\text{cm}^{-1}$, and the intensity of laser excitation immediately before the sample was $\sim 500\,\mu$W.

The dependences of the magnetization of powdered samples on temperature $M(T)$ were measured using a vibration magnetometer of the CFMS multifunctional cryomagnetic measuring system from Cryogenic Ltd, UK. The dependences $M(T)$ were measured in the ZFC mode (sample pre-cooled in a zero magnetic field) and FC mode (sample pre-cooled in a magnetic field of $H = 10$ kOe) in the temperature range of $T = 2-400$ K in a magnetic field of $H = 1$ kOe.

2. Results and discussion

2.1. Transmission electron microscopy (TEM)

Figure 1 shows TEM images of powdered samples of $La_{0.5}Sr_{0.5}FeO_{3-\gamma}$ synthesized at a temperature of 1100°C (50Sr−1100C). Large agglomerates of arbitrary shape, consisting of irregularly shaped particles tightly adjacent to each other, are observed in the sample structure. The average particle size was determined based on 50−100 particles. The size of the agglomerates recorded by the TEM method is in the range of $1.1-7\,\mu$m (average size $\sim 2.7\,\mu$m). The diffraction pattern (Figure 1, *c*) obtained from the observed agglomerates is close to annular and consists of separate bright reflections, which is characteristic of an accumulation of particles larger than 50 nm belonging to the same phase. According to the dark-field images (Figure 1, *b*) acquired in reflexes that correspond to the interplane distances $d_1 \sim 3.88$ Å and $d_2 \sim 2.74$ Å, which have close values to d_{012} and d_{104} (and d_{110}) rhombohedral $La_{0.5}Sr_{0.5}FeO_{3-\gamma}$, respectively, the size of the majority of particles is distributed in the range of 100−230 nm, and the measured average grain size in agglomerates is about 165 nm.

According to TEM data, the sample synthesized at a temperature of 1300°C (50Sr−1300C) contains only large particles with an average size of about $1.6\,\mu$m (Figure 2). The diffraction pattern (Figure 2, *c*) obtained from the observed particles is point-like, typical of the monocrystalline phase. The entire particle is illuminated on dark-field

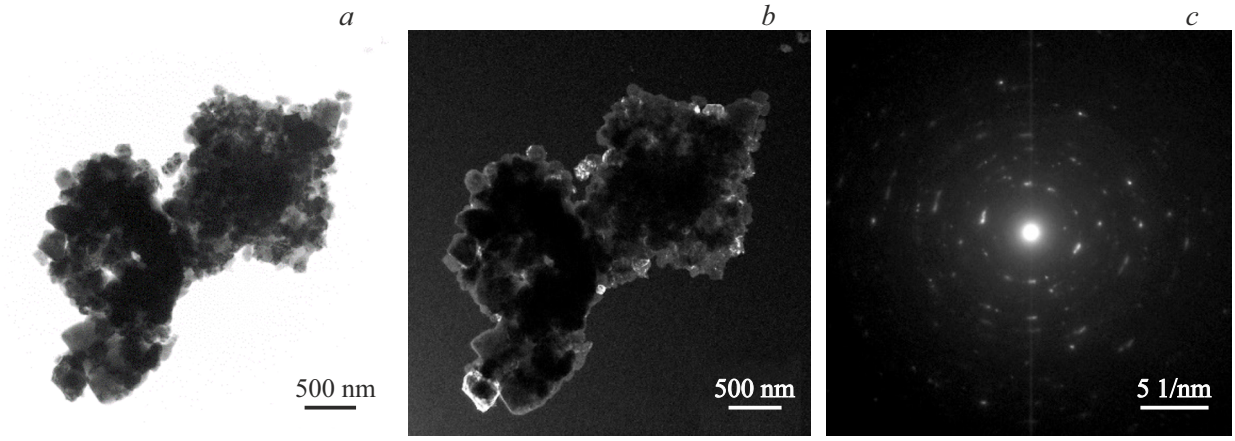

Figure 1. Bright-field (a), dark-field (b) TEM images and diffraction pattern (c) of a typical agglomerate in the initial sample 50Sr−1100C.

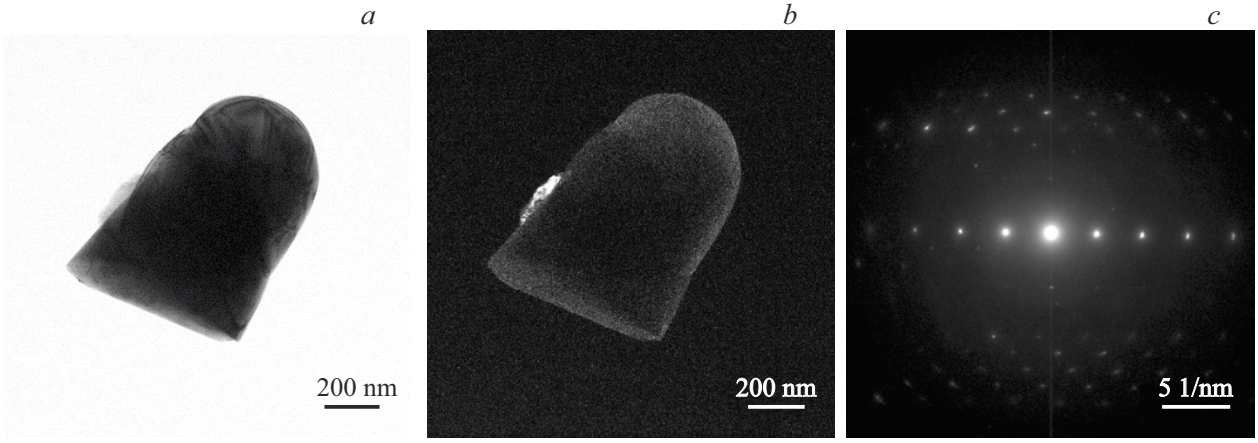

Figure 2. Bright-field (a), dark-field (b) TEM images and diffraction pattern (c) of a typical particle in the initial sample 50Sr−1300C.

(Figure 2, b) TEM images (Figure 2, b), which also indicates a homogeneous and monocrystalline structure.

TEM mapping with EDS was performed for a more complete characterization of the structure of sample 50Sr−1300C. The mapping results are provided in Figure 3 and show that the distribution of each element, including La, Sr, Fe, and O, is fairly uniform in large agglomerations as a result of synthesis at 1300°C.

A significant increase of the particle size is observed in a sample annealed in vacuum at 650°C for 8 hours (50Sr−1300C−650AV−8h). A TEM image of a typical particle is shown in Figure 4, a. According to TEM data, the size of such particles is in the range of $1-5.5\,\mu$m, which indicates its increase by almost half compared to the sample without annealing. The diffraction pattern obtained from the observed particles is point-like, typical of the monocrystalline phase (Figure 4, insert).

When the annealing time is increased to 10 hours, sufficiently large particles are observed in sample 50Sr−1300C−650AV−10h. The TEM image typical of this sample is shown in the figure (Figure 4, b). According to TEM data, the size of most particles is in the range of $1.1-11\,\mu$m with an average size of about $5.5\,\mu$m, large particles with size of $20-30\,\mu$m are also present in the sample. The diffraction pattern obtained from the observed agglomerates is point-like, typical of the monocrystalline phase (Figure 4, b, inset).

2.2. X-ray data

Results of X-ray diffraction analysis of ferrite $La_{0.5}Sr_{0.5}FeO_{3-\gamma}$ synthesized at 1100°C (sample 50Sr−1100C) and subsequently annealed in vacuum at temperatures of 200−650°C, are described in detail in Ref. [6]. It was shown that the initial compound has a rhombohedral structure, the parameters of the cell and, accordingly, its volume monotonously increase with the increase of the vacuum annealing temperature, while the rhombohedral angle α decreases. Annealing at a temperature of 650°C for 10 hours leads to the final transition of the lattice to a cubic one with the parameter $a = 3.914(1)$ Å. Figure 5, a shows the dependence of the

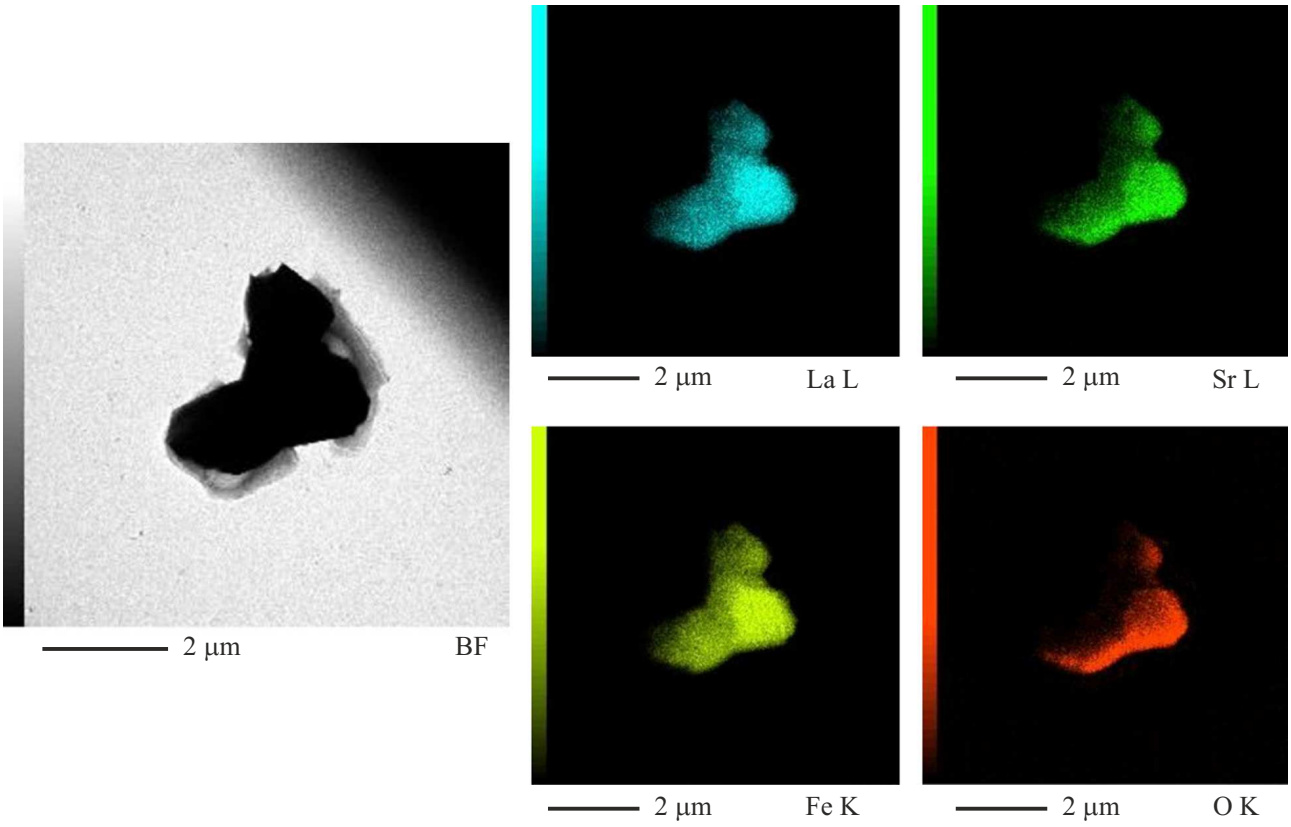

Figure 3. La, Sr, Fe, and O distribution pattern in powder 50Sr−1300C, acquired by TEM with EDS.

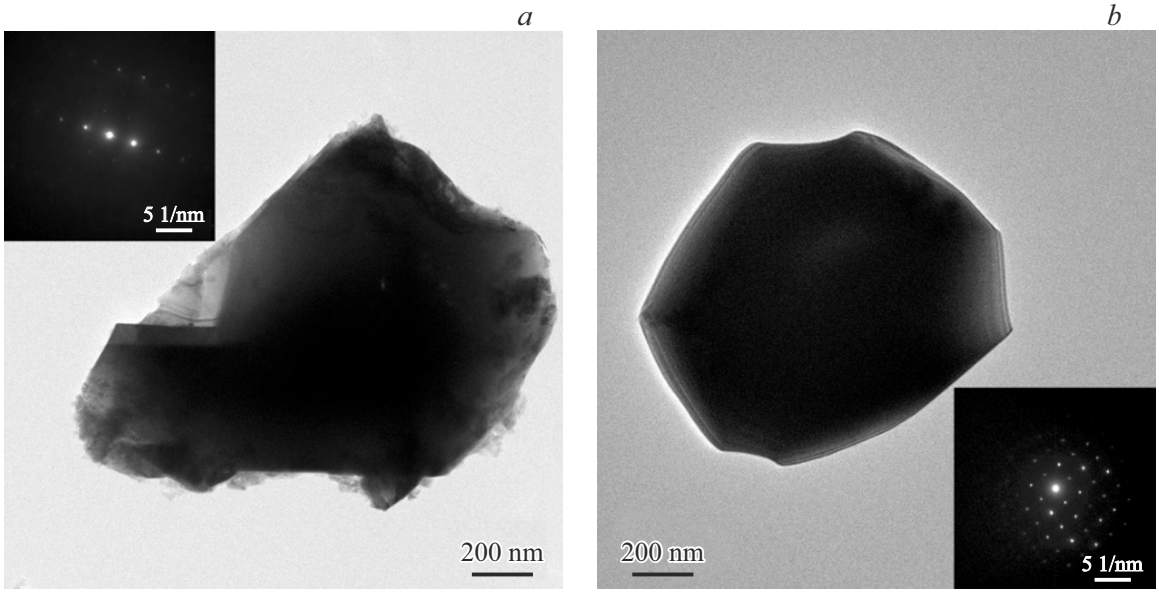

Figure 4. TEM images of observed particles and diffraction patterns (inserts) in samples 50Sr−1300C−650AV−8h (*a*) and 50Sr−1300C−650AV−10h (*b*).

crystal lattice volume of the initial sample 50Sr−1100C, assigned to a single pseudocubic perovskite cell, on the vacuum annealing temperature (T_{ann}). In addition, it was observed that the diffraction lines on the diffraction patterns of all samples, except those annealed at 650°C, are broadened. In the case of the initial sample, this is attributable to the small grain size, which is confirmed by the results of electron microscopic studies, in other cases,

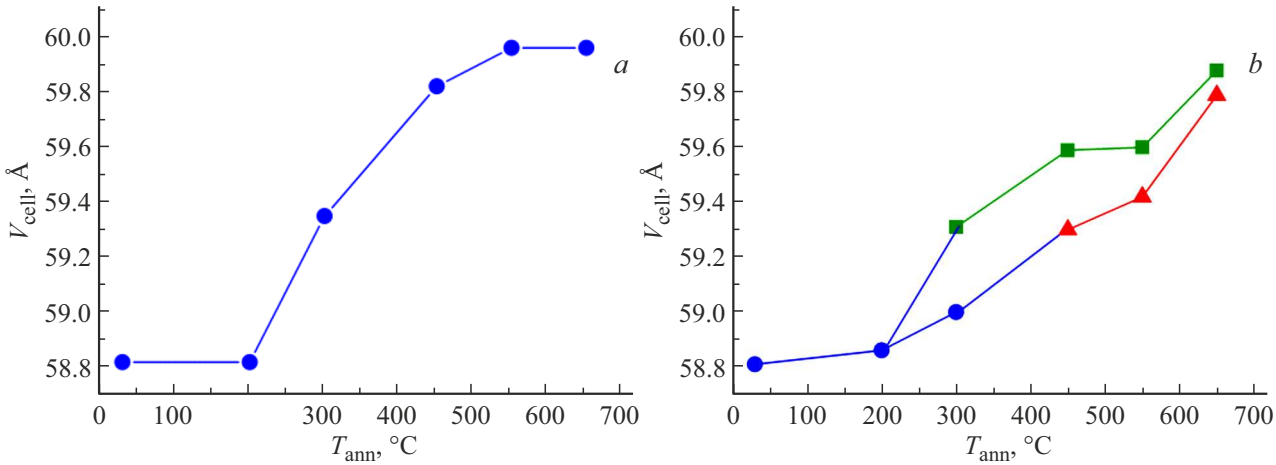

Figure 5. Temperature dependences of the crystal lattice volume per perovskite cell (V_{cell}): *a* — for sample 50Sr−1100C *b* — for sample 50Sr−1300C. V_{cell} for rhombohedral (in blue) and cubic (in green and red) phases in the sample.

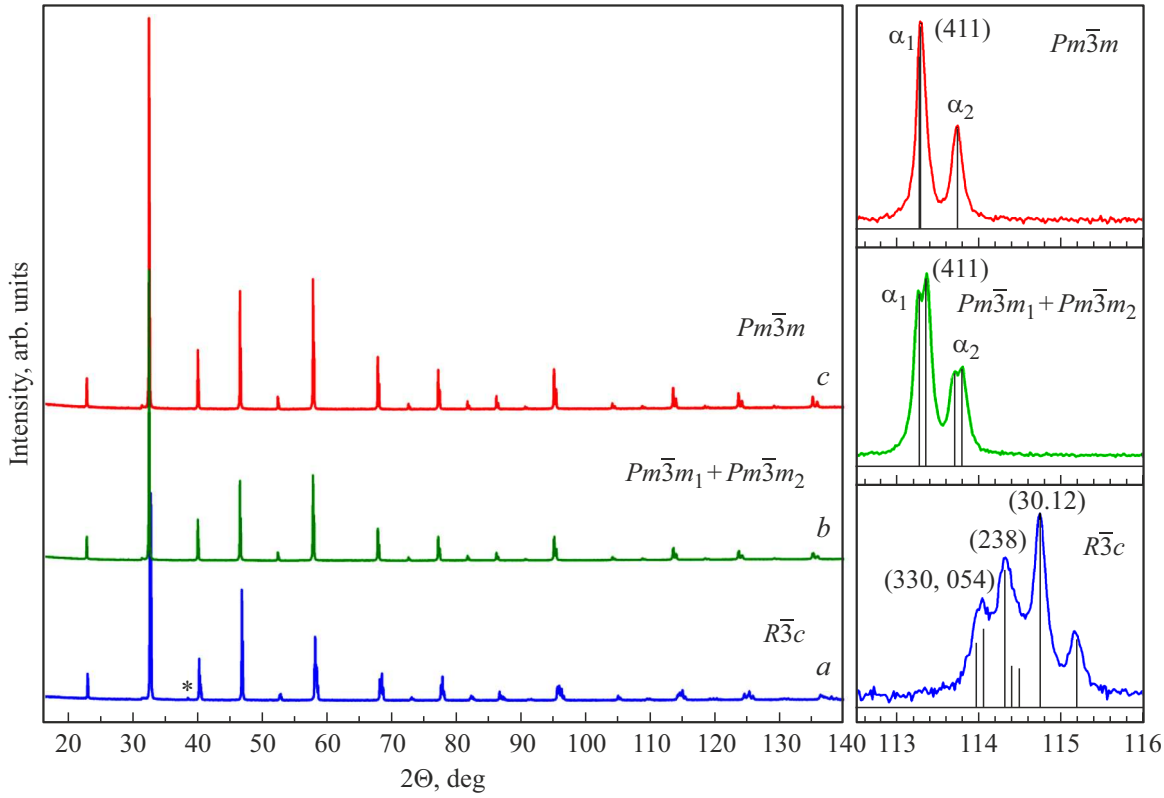

Figure 6. Diffraction patterns of samples 50Sr−1300C: initial sample (*a*); sample after annealing at 650°C for 8 hours (*b*) and 10 hours (*c*). The right panel shows the corresponding fragments of diffraction spectra in a limited angular range. The symbol (*) indicates the diffraction line (113) of the rhombohedral phase $R\bar{3}c$.

it may be attributable to the uneven distribution of oxygen after vacuum annealing.

The initial sample 50Sr−1300C also has a rhombohedral structure (e.g. $R\bar{3}c$, $a = 5.511(1)$ Å, $c = 13.415(2)$ Å in hexagonal axes or $a = 5.488(1)$ Å, $\alpha = 60.28(1)$ in rhombohedral axes). The diffraction lines of the spectrum of the initial sample (Figure 6, *a*), unlike sample 50Sr−1100C, are rather narrow and well resolved, which indicates a large grain size. This fact is confirmed by the results of TEM, according to which the average grain size in the initial sample 50Sr−1300C is 1.6 μm and is an order of magnitude larger than the average grain size in sample 50Sr−1100C.

Diffraction pattern of sample 50Sr−1300C after vacuum annealing at 200°C almost does not change and begins

to change only after annealing at 300°C. This spectrum is best described by a two-phase mixture that contains a cubic phase ($Pm\bar{3}m$) with $a = 3.900(1)$ Å in addition to the initial rhombohedral phase (with $a = 5.513(1)$ Å, $c = 13.447(2)$ Å). The crystal lattices of these phases are close, as a result of which the diffraction lines largely overlap. A further increase in the annealing temperature T_{ann} results in an increase in the lattice parameters of both phases and, accordingly, an increase in the volume of crystal cells.

Figure 5, *b* shows the dependences of the volume per perovskite cell (V_{cell}) on the vacuum annealing temperature (T_{ann}) for the rhombohedral and cubic phases composing a two-phase mixture in sample 50Sr−1300C. As can be seen, the cell volume of the cubic phase significantly exceeds the cell volume of the rhombohedral phase, and the volumes increase monotonously for both phases with the growth of T_{ann}. The calculation of the parameters of the crystal cell of phase $R\bar{3}c$ in a rhombohedral setup also shows a monotonous decrease in the angle α, which means a decrease in rhombohedral distortion and a restructuring of the rhombohedral lattice into a cubic lattice, as in the case of sample 50Sr−1100C. The angle α is almost equal to 60.00° already at annealing temperatures of 450 and 550°C, and the corresponding spectra are well described by two cubic lattices with different parameters. The weak diffraction line (113) at $2\Theta \approx 38.4°$ (marked with the symbol (∗) in Figure 6, *a*), which is not present in these spectra, can serve as a marker for the presence of a rhombohedral structure. It should be noted that due to the proximity of rhombohedral and cubic structures, as well as the superposition of their diffraction lines, the accuracy of determination of the structural parameters is not high. The diffraction lines are significantly widened compared to the original sample. Taking into account the TEM data, according to which the crystallite size increases in case of annealing, it can be assumed that this broadening is not attributable to the small grain size, but to the imperfection of the structure at the time of its active restructuring in case of oxygen removal at temperatures of 450−550°C, as well as the uneven distribution of oxygen over the volume of the crystallites.

Thus, it can be concluded that the annealed sample 50Sr−1300C contains two phases, the volume of which increases in case of vacuum annealing, in addition, the rhombohedral structure of one of these phases is transformed into a cubic structure in parallel.

At the first glance, 8 hour vacuum annealing at temperature of 650°C leads to the same result as in the case of sample 50Sr−1100C — the final transition to the cubic phase. However, a more thorough analysis of the spectrum (Figure 6, *b*, right panel) reveals a feature at the far corners of the diffraction: it is noticeable that each diffraction line consists of two. This is explained by the presence in the sample of two cubic lattices with a very small difference in parameter, $a_1 = 3.910(1)$ Å and $a_2 = 3.912(1)$ Å, their volumes are shown in Figure 5, *b*. When the annealing duration is increased to 10 hours at the same temperature of 650°C the entire sample is transformed into one cubic phase with $a = 3.912(1)$ Å (Figure 6, *c*); there is no bifurcation of lines in this case as can be seen in the right panel of the figure.

Since in this case the cell volume directly correlates with the oxygen content with a fixed La/Sr ratio, but varying amounts of Fe^{4+} and oxygen in the lattice (the lower the oxygen content is, the larger is the volume), it can be assumed that the sample annealed for 8 hours consists of two parts with different oxygen content, which equalizes with an increase in the annealing time to 10 hours. The difference may be related to the large size of the grains and their large size spread: the diffusion paths in smaller grains are shorter, and oxygen is released faster from them.

The following general observations can be made based on the comparison of the results obtained on samples with different synthesis temperatures (50Sr−1100C and 50Sr−1300C): the initial samples have approximately the same lattice volume per cell; the volume of both cubic and rhombohedral crystal cells increases as the temperature of vacuum annealing increases. The difference is that for the sample 50Sr−1100C, the volume with the annealing temperature grows faster than for 50Sr−1300C, and the cell parameters for the resulting cubic phase, which ends the structural transformation in both samples, differ by two units in the third sign. Moreover, this parameter is higher for the sample 50Sr−1100C, which probably corresponds to a lower oxygen concentration in the lattice. All these facts fit into the explanation related to the grain size in samples 50Sr−1100C and 50Sr−1300C.

2.3. Mössbauer data

2.3.1. Measurements at 300 K

All valence states of Fe and their relative amounts can be determined using Mössbauer spectroscopy. After that, the amount of oxygen and oxygen vacancies in the sample is determined with good accuracy. All parameters were determined in our study in Ref. [6] for sample 50Sr−1100C before annealing and after vacuum annealing in the temperature range of 200−650°C. The study of the sample 50Sr−1300C before annealing and after vacuum annealing at different temperatures was conducted using the same procedure.

The method of restoring the distribution of the spectrum parameters was used to process the spectra.

The initial sample 50Sr−1300C, like sample 50Sr−1100C, is paramagnetic at 300 K, their spectra practically do not differ from each other and are described by a quadrupole doublet. The values of isomer shifts (0.14−0.18 mm/s) indicate that Fe ions are in an average valence state, i.e. with a fractional degree of oxidation between 4+ and 3+. This state of Fe ions is attributable to the rapid (with a characteristic time of $< 10^{-8}$ s) electron transfer between Fe^{3+} and Fe^{4+} ions at 300 K, therefore, Fe^{4+} ions in substituted ferrites are not observed in the Mössbauer spectra measured at 300 K [7–9].

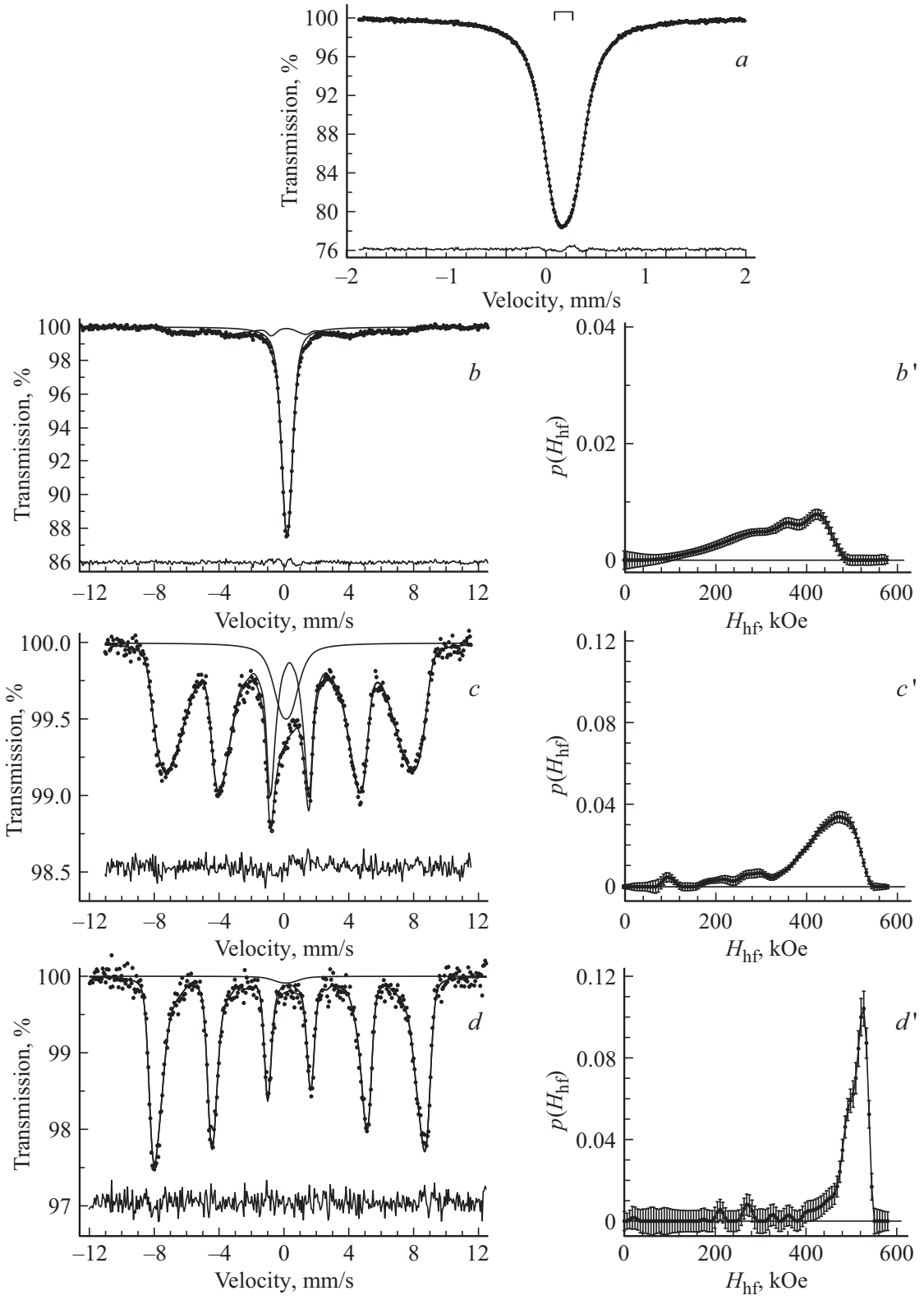

Figure 7. Results of fitting of the 300 K Mössbauer spectra of the initial sample 50Sr−1300C (a) and samples annealed in vacuum at temperatures T_{ann} 300 (b), 550 (c) and 650°C (d) for 8 hours and the results of reconstruction of the distributions $p(H_{hf})$ of the hyperfine magnetic field H_{hf}, taking into account the paramagnetic contribution (b', c', d'). The difference spectra are shown under each spectrum.

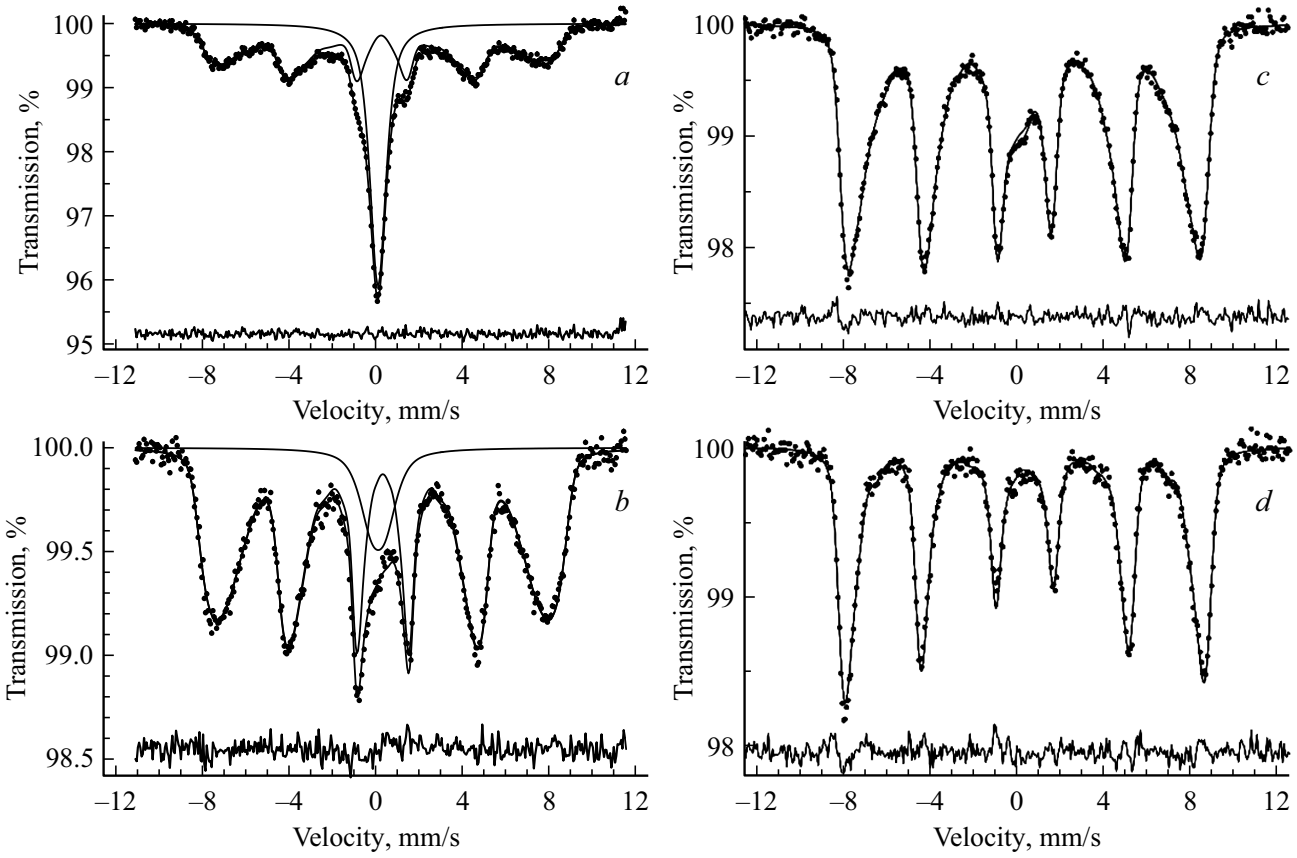

Figure 8. 300 K Mössbauer spectra of samples 50Sr−1300C (*a, b*) and 50Sr−1100C (*c, d*) annealed in vacuum at T_{ann} 450 (*a, c*) and 550°C (*b, d*).

The line widths of the sextets in sample 50Sr−1300C with the growth of T_{ann} are noticeably larger than in sample 50Sr−1100C. The lines strongly narrow after annealing at 650° for 10 h. It can be assumed that this behavior in sample 50Sr−1300C is attributable to the formation of two phases in case of annealing at a temperature above 200°C: cubic and rhombohedral.

The spectrum of sample 50Sr−1300C annealed at 550°C is similar to that of sample 50Sr−1100C annealed at 450°C (Figure 8), i.e., the transition of sample 50Sr−1300C to the magnetically ordered state is delayed in case of vacuum annealing compared to 50Sr−1100C. This can be explained by the large grain size of sample 50Sr−1300C, which leads to a decrease in the oxygen diffusion rate and its slower release from the lattice.

2.3.2. Measurements at 85 K

Mössbauer studies were performed at 85 K to obtain unambiguous information about the presence, quantity, and behavior of Fe^{4+} ions, the number of subspectra associated with the effect of La substitution for Sr, and the effect of oxygen vacancies. The spectra were processed and analyzed by the method of model fitting.

The 85 K Mössbauer spectra of the initial sample 50Sr−1300C and samples after a series of vacuum annealing are shown in Figure 9. They comprise a set of several magnetic subspectra, one of which, with a smaller isomer shift (-0.06 ± 0.03 mm/s) and an hyperfine magnetic field (264.4 ± 2.4 kOe), can be attributed to Fe^{4+} ions, and the others belong to Fe^{3+} ions with different local environments. The spectra of all samples measured at 85 K demonstrate that the averaged valence state does not appear, i.e., the electron transfer process between Fe^{3+} and Fe^{4+} ions freezes with a decrease in temperature. The presence of several subspectra in the spectra for Fe^{3+} ions is associated with the presence of different numbers of oxygen vacancies and Fe^{4+} ions in the nearest environment of these ions, i.e. with the formation of different types of local environment of Fe^{3+} ions. In this case, the area of each subspectrum is proportional to the fraction of the corresponding state of the Fe ion (taking into account the valence, and the type of local environment for Fe^{3+} ion). The spectra were fitted taking into account the possible number of oxygen vacancies and Fe^{4+} ions in the local environment of Fe^{3+} until the best difference spectrum was obtained, which generally corresponded to five subspectra for Fe^{3+} and one subspectra for Fe^{4+} (Figure 9). Figure 9 shows that vacuum annealing of the initial samples leads to a decrease in the proportion of Fe^{4+} ions, to an increase in the number of oxygen vacancies and, consequently, to a redistribution of the areas of the subspectra of Fe^{3+}

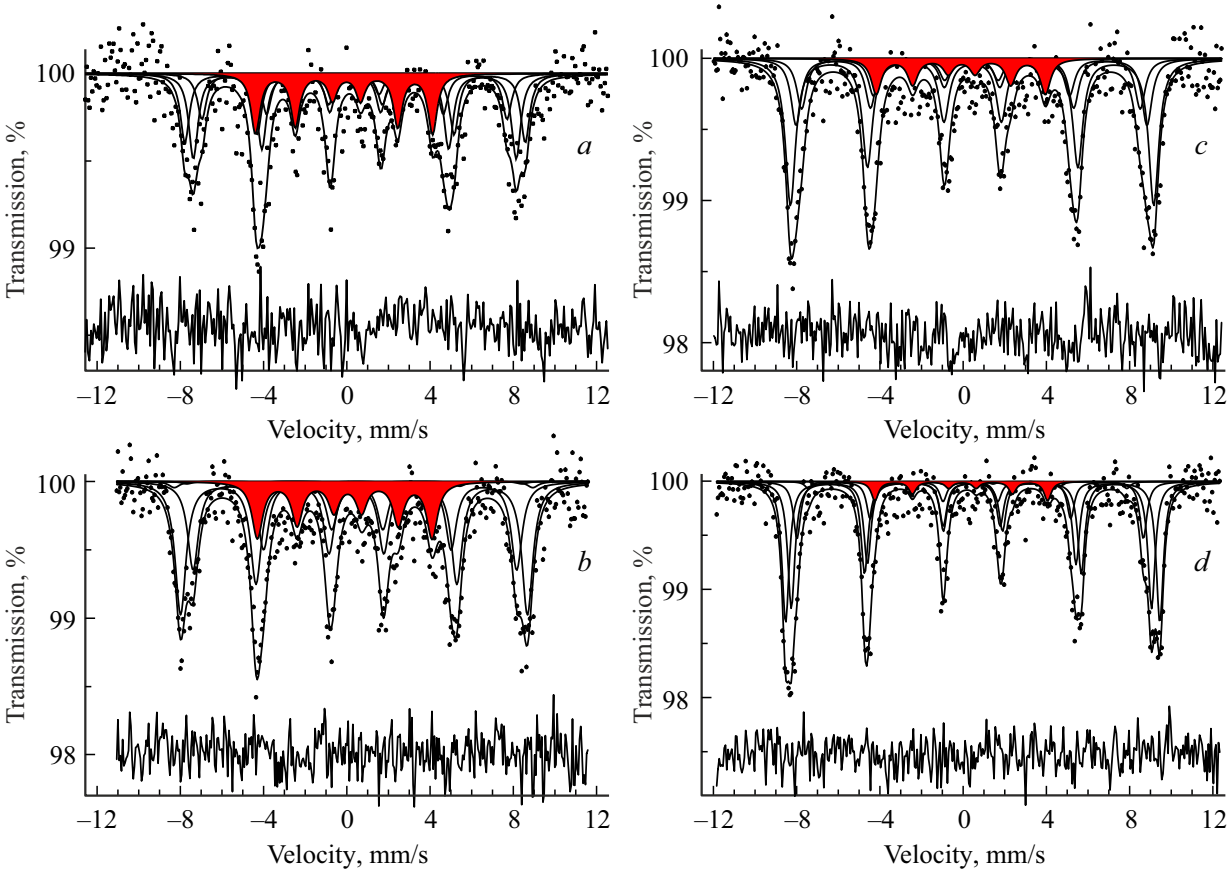

Figure 9. Results of model fitting of the 85 K Mössbauer spectra of 50Sr−1300C samples: initial (*a*) and annealed in vacuum at temperatures of 300 (*b*), 550 (it c) and 650°C (*d*) for 8 hours. The subspectrum of Fe^{4+} ions is highlighted by red color. The difference spectrum between the experimental and calculated values of the areas in the spectrum is shown under each spectrum.

ions. Knowing the number of Fe^{4+} (y), the number of oxygen vacancies ($\gamma = (0.5 - y)/2$) and oxygen ions ($3 - \gamma = (5.5 + y)/2$) in samples can be determined from considerations of electroneutrality according to the chemical formula $La^{3+}_{0.5}Sr^{2+}_{0.5}Fe^{3+}_{1-y}Fe^{4+}_{y}O^{2-}_{3-\gamma}$.

The dependences of the number of Fe^{4+} ions, as well as oxygen vacancies and oxygen ions per formula unit on the annealing temperature T_{ann} for samples 50Sr−1300C and 50Sr−1100C are shown in Figure 10.

As can be seen in Figure 10, *a*, the transition from Fe^{4+} to Fe^{3+} in sample 50Sr−1300C is slower than in 50Sr−1100C. Moreover, the number of oxygen ions is slightly higher in the annealed sample 50Sr−1300C−650AV−8h compared to the sample 50Sr−1100C−650AV (Figure 10, *b*), which correlates with the presence of a residual fraction of Fe^{4+} ions (4−5%). Both of these facts can be explained by the difference in grain sizes of samples 50Sr−1300C and 50Sr−1100C: the grain size of the initial sample 50Sr−1300C is an order of magnitude larger than in sample 50Sr−1100C according to electron microscopy data. Therefore, oxygen escapes from the lattice more slowly in case of the vacuum annealing of sample 50Sr−1300C. And, accordingly, the transition from Fe^{4+} to Fe^{3+} is slower.

Based on the Mössbauer data, it should be noted that the initial (original) and final (annealed at 650°C) states of samples 50Sr−1100C and 50Sr−1300C have a little difference from each other. The differences appear on the path of transition from the initial state to the final state in [5 case of vacuum annealing.

The Mössbauer data can be used to both calculate the average macroscopic characteristics of the compound, such as the fraction of Fe^{4+} and oxygen concentration, and to obtain information about the structure at the local level. The dependence of the parameters of each individual subspectrum of Fe^{3+} ions on the number of Fe^{4+} ions and vacancies in the nearest environment allows it to be associated with a specific variant of such an environment (a set of weakened or broken exchange bonds). The analysis of the areas of the subspectra makes it possible to estimate the distribution of such defects in the lattice.

Let's introduce the number m of broken or weakened exchange bonds of Fe^{3+} ion. The value $m = 0$ means that the Fe^{3+} ion in the nearest octahedral environment has all six exchange bonds $Fe^{3+}-O^{2-}-Fe^{3+}$, i. e. there are no oxygen vacancies and Fe^{4+} ions. The dependences of the areas of the subspectra of Fe^{3+} on T_{ann} of samples 50Sr−1100C for different values of m were obtained in

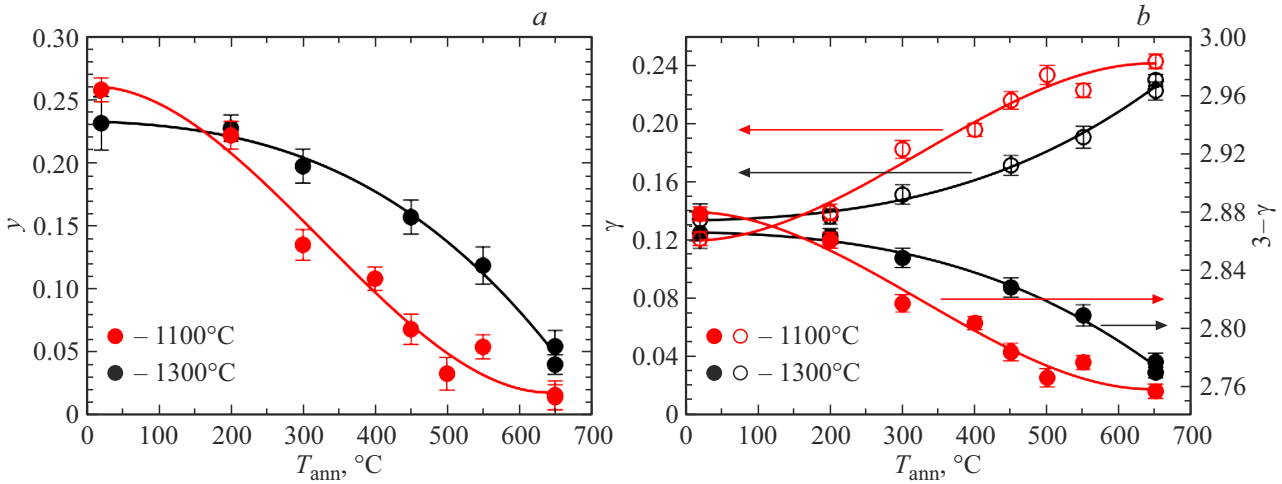

Figure 10. Dependences of the number of Fe^{4+} ions (y) (a), the number of oxygen vacancies (γ) (b) and the number of oxygen ions ($3-\gamma$) (b) per formula unit on the annealing temperature T_{ann} of samples 50Sr−1300C and 50Sr−1100C.

Ref. [6]. A similar analysis was performed for samples 50Sr−1300C in this study. These data can be used to construct and analyze their dependences on the number m for the initial samples 50Sr−1300C and 50Sr−1100C and the samples annealed at 650°C for 10 hours (Figure 11).

In the initial samples, the area of the subspectra corresponding to the state $m = 0$ (absence of vacancies and Fe^{4+} ions in the nearest environment of Fe^{3+} ion) is low for the sample 50Sr−1100C ($\sim$ 12%) and significantly greater for the sample 50Sr−1300C ($\sim$ 34%). The subspectra have the maximum area with $m = 2$ for 50Sr−1100C ($\sim$ 33%) and with $m = 1$ for 50Sr−1300C ($\sim$ 43%). Subspectra of samples annealed at 650°C have a maximum area at $m = 0$: $\sim$ 56% for 50Sr−1100C and $\sim$ 43% for 50Sr−1300C. Thus, the contributions of the subspectra of sample 50Sr 1100C before annealing and after annealing at 650°C are very different from each other at $m = 0$ (six exchange bonds $Fe^{3+}-O^{2-}-Fe^{3+}$), whereas this difference is small for samples 50Sr−1300C. As the number m increases, the areas of the subspectra significantly decrease and tend to zero. It should be noted that the course of the curves insignificantly differs for sample 50Sr−1300C before annealing and after annealing at 650°C compared to the curves for samples 50Sr−1100C (Figure 11).

The above is well confirmed by the results of calculation of the hyperfine magnetic field $H_{hf}(Fe^{3+})$ averaged over all subspectra of Fe^{3+} ions, depending on the temperature of vacuum annealing T_{ann} for both samples (50Sr−1100C and 50Sr−1300C) (Figure 12, a). The dependences of the average areas of the subspectra of Fe^{3+} ions on T_{ann} are shown in Figure 12, b. The increase in fields $H_{hf}(Fe^{3+})$ and the areas of subspectra of Fe^{3+} ions with an increase in T_{ann} is attributable to an increase in the number of exchange bonds for Fe^{3+}, a decrease in the number of Fe^{4+} ions and an increase in Néel temperature T_N (see below).

Thus, subspectra with $m = 1$ and 2 make the main contribution to the Mössbauer spectra in initial samples 50Sr−1300C and 50Sr−1100C. This means that most of the Fe ions in the initial samples have one or two broken (presence of oxygen vacancies) or weakened (presence of Fe^{4+} ions) exchange bonds in their local environment. Subspectra with $m = 0$ (six exchange bonds $Fe^{3+}-O^{2-}-Fe^{3+}$) when there are no Fe^{4+} ions, no oxygen vacancies make the main contribution to the spectra in the annealed samples. This indicates that the structure becomes less defective in case of annealing, despite the increase in the number of vacancies.

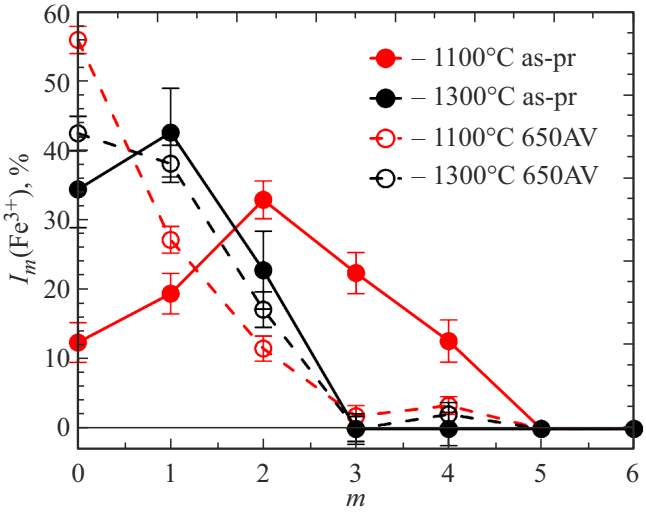

Figure 11. Dependences of the relative area of the subspectra I_m for Fe^{3+} ions on the number m of broken or weakened exchange bonds for the initial (as-pr.) and annealed at 650°C samples 50Sr−1100C and 50Sr−1300C.

2.4. Raman scattering data

The formation of two phases in case of vacuum annealing above 200°C in samples 50Sr−1300C is also confirmed by raman scattering (RS). Figure 13 shows the RS spectra

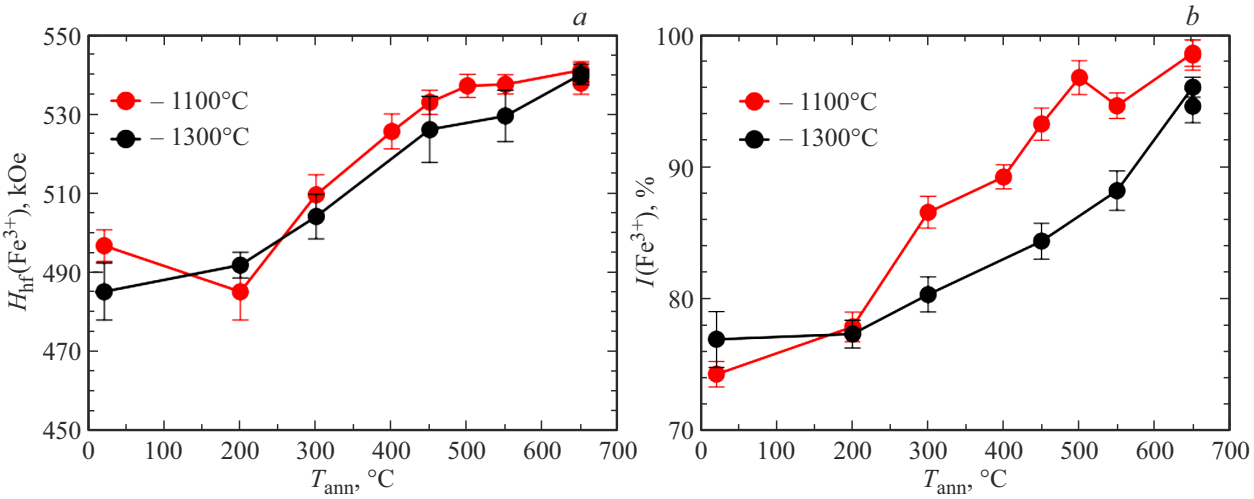

Figure 12. Dependences of the average values of hyperfine magnetic fields H_{hf} (Fe^{3+}) (*a*) and the areas of subspectra (*b*) for Fe^{3+} ions on the annealing temperature T_{ann} of samples 50Sr−1100C and 50Sr−1300C.

of samples annealed after synthesis at different vacuum annealing temperatures T_{ann}.

It is known that lines at frequencies below 1000 cm^{-1} in the RS spectra of orthoferrites $La_{1-x}Sr_xFeO_{3-y}$ are caused by phonon oscillations [10]. For instance, the strongest phonon mode at frequencies $\sim 660-700\,cm^{-1}$ describes in-phase oscillations of Fe−O bonds in the octahedron FeO_6, the so-called „breathing" octahedron mode [10]. It can be seen from Figure 13, *a* that intense phonon peaks are observed against an extended structureless background only in samples annealed at a temperature of $T^{\circ}_{ann} > 450°C$. The suppression of phonon modes in the RS spectra of substituted lanthanum orthoferrites annealed at lower temperatures indicates a significant proportion of Fe^{4+} ions in samples with low T_{ann}, as we showed in Ref. [11].

The strongest phonon mode at $\sim 660\,cm^{-1}$ of in-phase oscillations of the octahedron FeO_6 is abnormally broadened and has the doublet structure in samples with high synthesis temperature of 1300°C (50Sr−1300C) and annealing temperature of $T_{ann} = 550°C$ and 650°C (both for 8 hours and 10 hours), which is clearly visible after subtracting the linear background in the range of $500-850\,cm^{-1}$ and approximation by Gaussians (Figure 13, *b*). At the same time, the ratio R of intensities of I_{low} of low-energy ($E_1 \sim 627 \pm 2\,cm^{-1}$) and I_{high} — high-energy ($E_2 \sim 690 \pm 2\,cm^{-1}$) components of the RS spectrum in the sample after 8 hours of annealing at $T_{ann} = 650°C$ is significantly greater: $R = I_{low}/I_{high} \sim 0.43$ than in the sample after 10 hours of annealing: $R \sim 0.09 \pm 0.01$. It is natural to attribute the low-energy and high-energy components of the phonon mode at $\sim 660\,cm^{-1}$ to similar but different cubic crystalline phases identified by X-ray diffraction analysis. A significant attenuation of the low-energy component, by more than 3 times, in the sample after 10 hours of annealing is confirmed by X-ray diffraction analysis data indicating the disappearance of one of the cubic phases with the increase of the annealing time. For

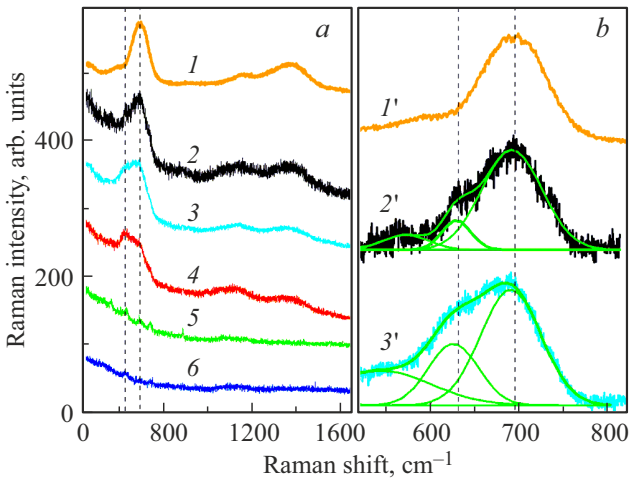

Figure 13. *a* — Raman scattering spectra of samples 50Sr−1300C (*2*–*6*, synthesis 1300°C) annealed in vacuum at $T_{ann} = 650°C$, 10 hours (*2*); 650°S, 8 hours (*3*); 550°C, 8 hours (*4*); 450°C, 8 hours (*5*) and 300°C, 8 hours (*6*). The spectra are shifted vertically. The dashed lines are drawn in the region of the strongest phonon mode $\sim 660-700\,cm^{-1}$. For comparison, the spectrum of the sample 50Sr−1100C (synthesis 1100°C) after annealing for 10 hours at 650°C (*1* and *1′*). *b* — RS spectra of samples with $T_{ann} = 650°C$, 10 hours (*2′*) and 650°C, 8 hours (*3′*) after subtracting the linear background at $500-850\,cm^{-1}$. Green lines — approximation by Gaussians.

comparison, Figure 13 shows the RS spectrum of sample 50Sr−1100C (*1* and *1′*) after annealing at 650°C, which has no pronounced phonon mode structure at $\sim 660\,cm^{-1}$, and the mode itself, which is active in the RS spectrum, is significantly narrower. Thus, RS spectroscopy confirms the appearance of a specific two-phase state with a cubic crystal structure in sample 50Sr−1300C in case of vacuum annealing.

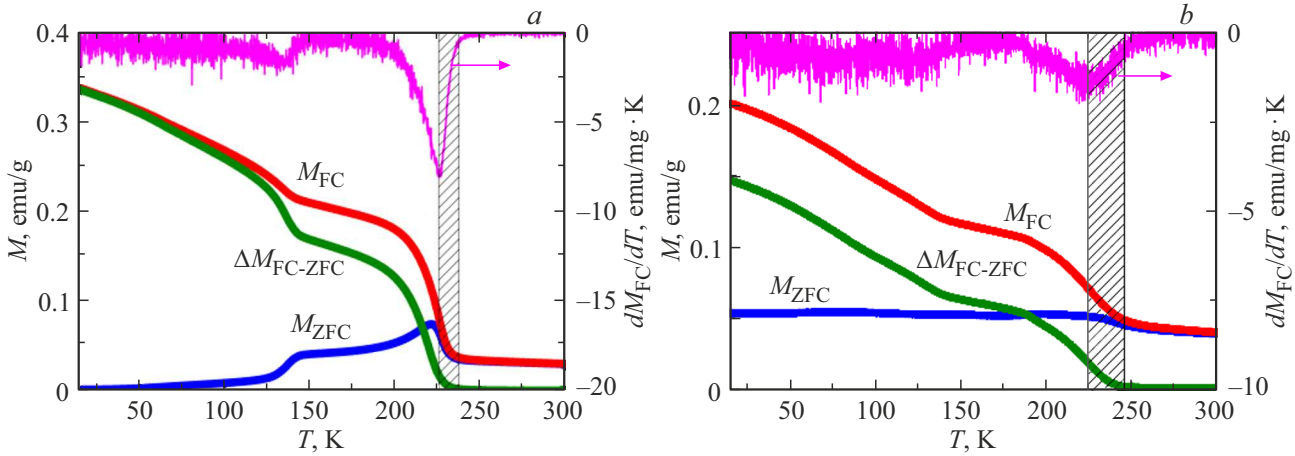

Figure 14. Dependences of the magnetization of the initial samples 50Sr−1300C (a) and 50Sr−1100C (b) on temperature $M(T)$. The red curves correspond to FC mode, the blue ones correspond to ZFC mode, the green color shows the difference of the curves $M_{FC} - M_{ZFC} = \Delta M_{FC-ZFC}$, the purple curve corresponds to the derivative dM_{FC}/dT. The hatching shows the critical areas.

It should be noted that the presence of a pronounced broad peak of two-magnon scattering at $\sim 1350\,cm^{-1}$ in the RS spectra of samples annealed after synthesis at $T_{ann} = 550°C$ and 650°C (Figure 13, a) indicates the antiferromagnetic type of ordering in them at room temperature [12]. A similar but stronger two-magnon scattering line is observed in unsubstituted lanthanum ferrite $LaFeO_3$ with the highest Néel temperature $T_N = 740\,K$ and in the brownmillerite phase $SrFeO_{2.5}$ with $T_N = 670\,K$ [13]. In addition to the two-magnon peak, there is also an intense two-phonon scattering line at $\sim 1150\,cm^{-1}$, which is manifested due to the strong coupling of the phonon and spin systems in these compounds [14].

2.5. Magnetic measurements

The magnetization curves of sample 50Sr−1300C have several temperature features. However, the Néel temperatures T_N and their dependence on the synthesis temperature and their change with the vacuum annealing are of the main interest in this study. A detailed analysis of the magnetization curves over the entire temperature range and related magnetic features will be presented in a separate paper, as was done for sample 50Sr−1100C synthesized and annealed in vacuum at 650°C [15]. Therefore, only the temperature regions corresponding to the transition to a magnetically ordered state at the Néel point are discussed below.

The temperature dependences of the magnetization $M(T)$, measured in the ZFC and FC modes, of the initial samples 50Sr−1300C and 50Sr−1100C are shown in Figure 14. The data for sample 50Sr−1100C, which we studied earlier, are taken from Ref. [15]. A characteristic temperature range of changes in the magnetic state of the sample (shown by hatching) in a relatively narrow range of $T = 226-233\,K$, which corresponds to the transition to a magnetically ordered state can be distinguished in Figure 14, a for sample 50Sr−1300C. A peak is observed on the curve M_{ZFC} at a temperature of $T_1 = 226 \pm 4\,K$, an inflection which is well visualized using the derivative dM_{FC}/dT is observed on the curve M_{FC} (Figure 14, a, purple curve). The difference between the curves $\Delta M_{FC-ZFC} = M_{FC} - M_{ZFC}$ turns to zero at temperature of $T_2 = 233 \pm 3\,K$, which corresponds to the final transition to the paramagnetic state (Figure 14, a, green curve). Taking into account the error $T_1 \approx T_2$. This means that the complete transition to a magnetically ordered state in the initial single-phase sample 50Sr−1300C occurs in the vicinity of $T_N \sim 230\,K$, the same as in the sample 50Sr−1100C (Figure 14, b) [15]. A slight broadening in the transition temperature range for sample 50Sr−1100C (Figure 14, b) may be attributable to an order of magnitude smaller grain size compared to sample 50Sr−1300C.

Magnetic measurements of sample 50Sr−1300C−450AV−8h were performed taking into account the X-ray and Mössbauer data on the presence of a two-phase state in this sample. The dependencies $M(T)$ of the annealed sample 50Sr−1300C−450AV−8h are shown in Figure 15, a. The region corresponding to the transition to a magnetically ordered state has a wide temperature range of $T = 255-305\,K$. A peak is observed on the curve M_{ZFC}, and an inflection is observed on the curve M_{FC} at a temperature of $T_1 = 255 \pm 5\,K$, which is well manifested on the derivative dM_{FC}/dT. The difference of the curves $\Delta M_{FC-ZFC} = M_{FC} - M_{ZFC}$ turns to zero at temperature of $T_2 = 305 \pm 5\,K$, which corresponds to the transition to the paramagnetic state. Such a wide transition region is probably attributable to the two-phase state of the sample, as well as the inhomogeneous distribution of oxygen over its volume and significant disordering of the structure at the time of its intensive restructuring.

The dependencies $M(T)$ of the annealed sample 50Sr−1300C−650AV−8h are shown in Figure 15, b. The region corresponding to the transition to a magnetically ordered state narrows and shifts towards higher temperatures

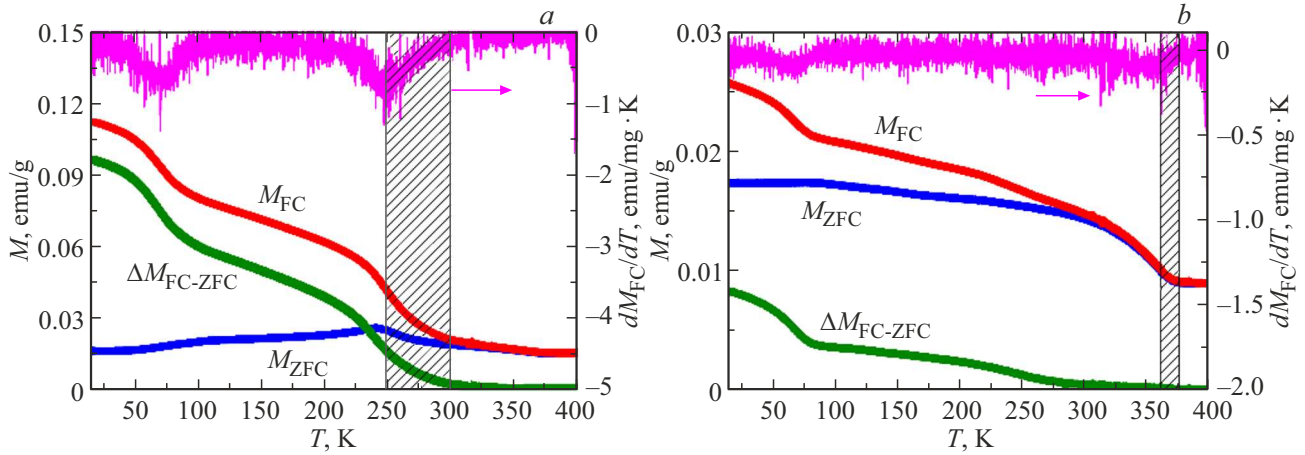

Figure 15. Temperature dependence of magnetization $M(T)$ of annealed samples 50Sr−1300C−450AV−8h (a) and 50Sr−1300C−650AV−8h (b). The red curves correspond to FC mode, the blue ones correspond to ZFC mode, the green color shows the difference of the curves $M_{FC} - M_{ZFC} = \Delta M_{FC-ZFC}$, the purple curve corresponds to the derivative dM_{FC}/dT. The hatching shows the critical areas.

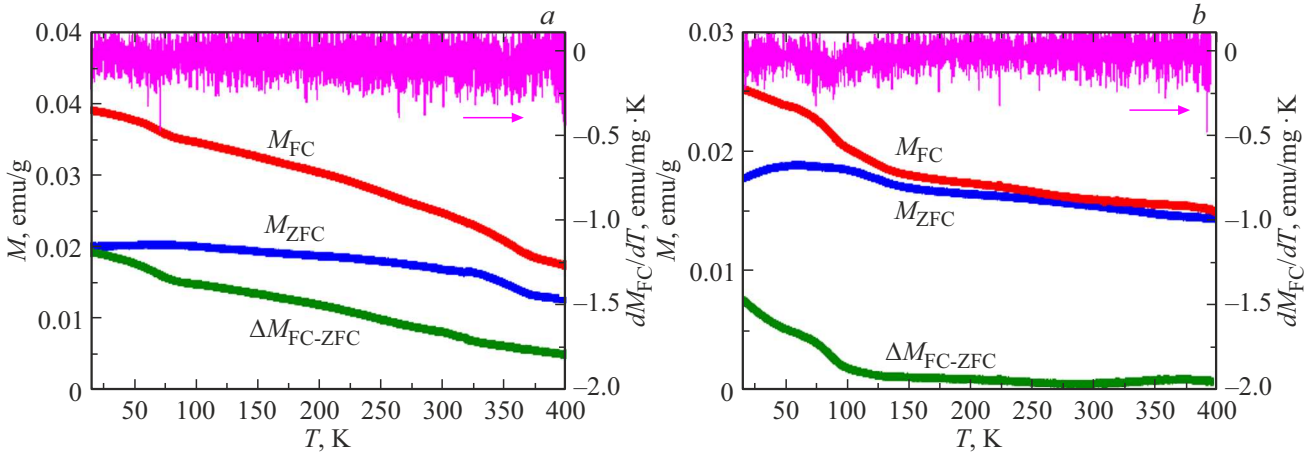

Figure 16. Magnetization dependences of annealed samples 50Sr−1300C−650AV−10h (a) and 50Sr−1100C−650AV−10h (b) on temperature $M(T)$. The red curves correspond to FC mode, the blue curves correspond to ZFC mode, the green color shows the difference of the curves $M_{FC} - M_{ZFC} = \Delta M_{FC-ZFC}$, the purple curve corresponds to the derivative dM_{FC}/dT. The hatching shows the critical areas.

$T = 360-370$ K. The inflection on the MFC curve occurs at a temperature of $T_1 = 360 \pm 5$ K and is well observed on the derivative dM_{FC}/dT. The difference of curves $\Delta M_{FC-ZFC} = M_{FC} - M_{ZFC}$ turns to zero at temperature $T_2 = 370 \pm 5$ K. It is important to note that increase in the vacuum annealing temperature to 650°C leads to a significant narrowing of the temperature range of the transition to a magnetically ordered state. Taking into account the error $T_N \approx 365$ K.

Figure 16 shows the curves $M(T)$ of annealed samples 50Sr−1300C−650AV−10h and 50Sr−1100C−650AV−10h, in which the region corresponding to the transition to a magnetically ordered state shifts towards temperatures above 400 K, exceeding the range available on the magnetometer. Peaks and inflections disappear on the MZFC and MFC curves, respectively, for the sample 50Sr−1300C−650AV−10h (Figure 16, a) up to 400 K. No features are observed on the derivative dM_{FC}/dT. The difference of the curves $\Delta M_{FC-ZFC} = M_{FC} - M_{ZFC}$ for the two samples in the considered temperature range does not become zero (Figure 16), i. e. the transition to the paramagnetic state in the samples occurs at temperatures above 400 K.

Thus, an increase of the vacuum annealing time of sample 50Sr−1300C by only 2 hours at constant temperature of 650°C leads to a noticeable increase in T_N. There is no broadening of the temperature range of the transition to the magnetically ordered state (Figure 16, a). The transition for sample 50Sr−1100C−650AV−10h also occurs at temperatures above 400 K (Figure 16, b) [15].

Thus, an increase in temperature in case of vacuum annealing of samples 50Sr−1300C and 50Sr−1100C leads

to a noticeable increase in T_N due to the mechanisms of redistribution of contributions of ferro- and antiferromagnetic channels to the resulting exchange and a shift in the balance towards increased antiferromagnetism. This is caused by a decrease in the proportion of Fe^{4+} ions in case of vacuum annealing, which is discussed in detail in our papers [15,16].

Both samples 50Sr−1300C and 50Sr−1100C, both in the initial state and annealed at 650°C for 10 hours, are single-phase, for this reason the temperature range of the transition to the magnetically ordered state is narrow on the dependences $M(T)$.

Noticeable difference in T_N of samples 50Sr−1300C annealed at 650°C for 8 and 10 hours (Figures 15, *b* and 16, *a*) is attributable to the fact that the two-phase state still remains in the sample and a small amount (5−6%) of Fe^{4+} ions remains after eight hours of annealing which significantly reduces T_N.

3. Conclusion

It follows from the analysis of the data obtained by the TEM method that the average grain size of the synthesized samples increases by almost an order of magnitude, from 165 nm to 1.6 μm (large monocrystalline particles are formed) with an increase in the temperature of the final annealing of the sol-gel synthesis from 1100 to 1300°C. The analysis of the TEM data shows that the average particle size of sample 50Sr−1300C annealed in vacuum at 650°C for 8 hours increases almost twice as compared with the original sample, and it increases approximately by 3.5 times in case of 10 hour-annealing.

The structure of sample 50Sr−1300C changes during vacuum annealing in a two-phase stage, with cubic and rhombohedral phases co-existing at low annealing temperatures, and two cubic phases in the higher temperature range. The volume of both cubic and rhombohedral crystal cells increases with the increase of temperature of vacuum annealing. The cell volume of sample 50Sr−1100C grows faster with the annealing temperature than the cell volume of sample 50Sr−1300C, which may be attributable to the difference in grain size.

The cell parameters for the resulting cubic phase differ, and for the sample 50Sr−1100C, this parameter is higher, which corresponds to a lower oxygen concentration in the lattice according to Mössbauer spectroscopy data. This fact also fits into the explanation related to the grain size in samples 50Sr−1100C and 50Sr−1300C.

The formation of two phases in case of annealing above 200°C and transition to a single phase at 650°C (10 hours) in the sample 50Sr−1300C can explain the initial noticeable broadening of the Mössbauer lines with the growth of T_{ann} and their narrowing after annealing at 650°C.

The number of valence states of Fe ions, the amount of oxygen, and vacancies in all samples were determined from the obtained Mesbauer data. The number of Fe^{4+} ions and oxygen ions is slightly higher for 50Sr−1100C in the initial samples. It is shown that most of the Fe ions in the initial samples have one or two defects in their local environment — a broken and/or weakened exchange bond. The proportion of Fe ions with a defective environment decreases in case of vacuum annealing, despite the increase in the number of vacancies and this effect is more pronounced for sample 50Sr−1100C. The oxygen content is slightly higher for 50Sr−1300C in samples annealed at 650°C. It was found that the oxygen release during vacuum annealing and, accordingly, the transition of Fe^{4+} to Fe^{3+} is more slow in samples synthesized at a higher temperature (1300°C). This is attributable to the large grain size in such samples.

RS spectroscopy confirms the occurrence of a two-phase state in samples 50Sr−1300C in case of vacuum annealing above 200°C, its transformation with an increase in the temperature of vacuum annealing and transition to a single-phase state at 650°C. The presence of a peak of two-magnon scattering in the RS spectra of vacuum-annealed samples indicates an antiferromagnetic type of ordering in them at room temperature.

It is shown that the Néel temperature T_N of samples 50Sr−1300C and 50Sr−1100C is approximately the same (230 K) in the initial state. Temperatures T_N of samples annealed at650°C in both cases are significantly higher in comparison with the initial samples (exceed 400 K). Using the example of sample 50Sr−1300C, it is shown that the temperature T_N markedly increases in case of vacuum annealing with the increase in annealing temperature (450 and 650°C) and duration (8 and 10 hours) which is a consequence of a shift of the balance towards increased antiferromagnetism associated with a decrease in the proportion of Fe^{4+} ions. Formation of a two-phase state in sample 50Sr−1300C in case of vacuum annealing below 650°C leads to a strong broadening of the temperature range of the transition to a magnetically ordered state based on the dependence $M(T)$. Transition to a single-phase state at 650°C greatly narrows this temperature range.

The results obtained by different methods correlate well with each other.

Acknowledgments

The authors are grateful to the Center for the Collective Use of Scientific Equipment of ISSP RAS for providing experimental facilities for conducting structural research.

Funding

The study was conducted under the State Assignments of Osipyan Institute of Solid State Physics RAS (075-00370-24-04) and Federal Research Center of Problems of Chemical Physics and Medicinal Chemistry RAS (124013100858-3). X-ray diffraction studies were performed using the equipment of the Collective Use Center of Osipyan Institute of Solid State Physics RAS.

Conflict of interest

The authors declare that they have no conflict of interest.

References

[1] S. Petrovic, A. Terlecki, L. Karanovic, P. Kirilov-Stefanov, M. Zduji, V. Dondur, D. Paneva, I. Mitov, V. Rakic. Appl. Catal. B. Environ. **79**, 186 (2008). https://doi.org/10.1016/J.APCATB.2007.10.022.
[2] J. Faye, A. Bayleta, M. Trentesauxb, S. Royera, F. Dumeignil, D. Duprez, S. Valange. Appl. Catal. B Environ. **126**, 134 (2012). https://doi.org/10.1016/J.APCATB.2012.07.001.
[3] E.K. Abdel-Khalek, D.A. Rayan, Ahmed.A. Askar, M.I.A. Abdel Maksoud, H.H. El-Bahnasawy. J. Sol-Gel Sci. Technol. **97**, 27 (2021). https://doi.org/10.1007/s10971-020-05431-8.
[4] J.B. Yang, W.B. Yelon, W.J. James, Z. Chu, M. Kornecki, Y.X. Xie, X.D. Zhou, H.U. Anderson, Amish G. Joshi, S.K. Malik. Phys. Rev. B **66**, 184415 (2002). https://doi.org/10.1103/PhysRevB.66.184415.
[5] M.E. Matsnev, V.S. Rusakov. AIP Conf. Proc. **1489**, 178 (2012). https://doi.org/10.1063/1.4759488.
[6] V. Sedykh, V. Rusakov, O. Rybchenko, A. Gapochka, K. Gavrilicheva, O. Barkalov, S. Zaitsev, V. Kulakov. Ceram. Int. **49**, *15*, 25640 (2023). https://doi.org/10.1016/j.ceramint.2023.05.105.
[7] P.D. Battle, N.C. Gibb, S. Nixon. J. Solid State Chem. **79**, 75 (1989). https://doi.org/10.1016/0022-4596(89)90252-1
[8] G. Li, L. Li, M. Zhao. Phys. Stat. Sol. B **197**, 165 (1996). https://doi.org/10.1002/pssb.2221970123
[9] P.D. Battle, T.C. Gibb, S. Nixon. J. Solid State Chem. **77**, 124 (1988). https://doi.org/10.1016/0022-4596(88)90099-0.
[10] M.C. Weber, M. Guennou, H.J. Zhao, J. Íñiguez, R. Vilarinho, A. Almeida, J.A. Moreira, J. Kreisel. Phys. Rev. B **94**, 214103 (2016). https://doi.org/10.1103/PhysRevB.94.214103.
[11] V. Sedykh, O. Rybchenko, V. Rusakov, S. Zaitsev, O. Barkalov, E. Postnova, T. Gubaidulina, D. Pchelina, V. Kulakov. J. Phys. Chem. Solids **171**, 111001 (2022). https://doi.org/10.1016/j.jpcs.2022.111001.
[12] G.B. Wright. Light Scattering Spectra of Solids. Springer Berlin, Heidelberg (1969). P. 763.
[13] O.I. Barkalov, S.V. Zaitsev, V.D. Sedykh. Solid State Commun. **354**, 114912 (2022). https://doi.org/10.1016/j.ssc.2022.114912.
[14] M.O. Ramirez, M. Krishnamurthi, S. Denev, A. Kumar, S.-Y. Yang, Y.-H. Chu, E. Saiz, J. Seidel, A.P. Pyatakov, A. Bush, D. Viehland, J. Orenstein, R. Ramesh, V. Gopalan. Appl. Phys. Lett. **92**, *2*, 022511 (2008). https://doi.org/10.1063/1.2829681.
[15] A.I. Dmitriev, S.V. Zaitsev, M.S. Dmitrieva, O.G. Rybchenko, V.D. Sedykh. FTT **66**, *3*, 386 (2024). (in Russian). https://doi.org/10.61011/FTT.2024.03.57479.1.
[16] A.I. Dmitriev, S.V. Zaitsev, M.S. Dmitrieva. Pis'ma v ZhTF **50**, *13*, 24 (2024). (in Russian). https://doi.org/10.61011/PJTF.2024.13.58163.19894.

Translated by A.Akhtyamov